34

SATELLITE & MESOMETEOROLOGY RESEARCH PROJECT

Department of the Geophysical Sciences
The University of Chicago

THE SCANNING PRINTER AND ITS APPLICATION TO DETAILED ANALYSIS OF SATELLITE RADIATION DATA

by

Tetsuya Fujita

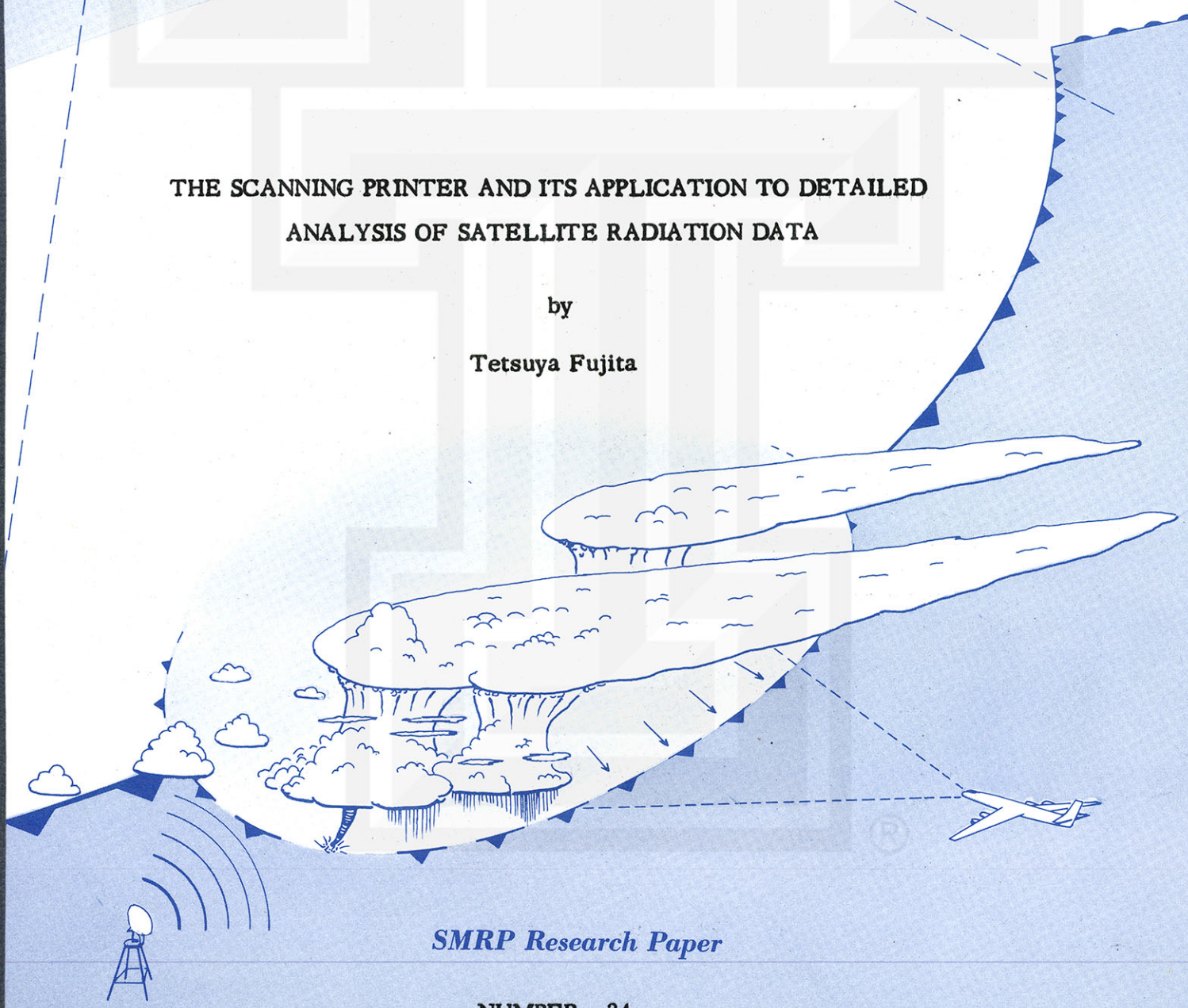

SMRP Research Paper

NUMBER 34

July 1964

MESOMETEOROLOGY PROJECT ---- RESEARCH PAPERS

1.* Report on the Chicago Tornado of March 4, 1961 - Rodger A. Brown and Tetsuya Fujita

2.* Index to the NSSP Surface Network - Tetsuya Fujita

3.* Outline of a Technique for Precise Rectification of Satellite Cloud Photographs - Tetsuya Fujita

4.* Horizontal Structure of Mountain Winds - Henry A. Brown

5.* An Investigation of Developmental Processes of the Wake Depression Through Excess Pressure Analysis of Nocturnal Showers - Joseph L. Goldman

6.* Precipitation in the 1960 Flagstaff Mesometeorological Network - Kenneth A. Styber

7.** On a Method of Single- and Dual-Image Photogrammetry of Panoramic Aerial Photographs - Tetsuya Fujita

8. A Review of Researches on Analytical Mesometeorology - Tetsuya Fujita

9. Meteorological Interpretations of Convective Nephsystems Appearing in TIROS Cloud Photographs - Tetsuya Fujita, Toshimitsu Ushijima, William A. Hass, and George T. Dellert, Jr.

10. Study of the Development of Prefrontal Squall-Systems Using NSSP Network Data - Joseph L. Goldman

11. Analysis of Selected Aircraft Data from NSSP Operation, 1962 - Tetsuya Fujita

12. Study of a Long Condensation Trail Photographed by TIROS I - Toshimitsu Ushijima

13. A Technique for Precise Analysis of Satellite Data; Volume I - Photogrammetry (Published as MSL Report No. 14) - Tetsuya Fujita

14. Investigation of a Summer Jet Stream Using TIROS and Aerological Data - Kozo Ninomiya

15. Outline of a Theory and Examples for Precise Analysis of Satellite Radiation Data - Tetsuya Fujita

* Out of print
** To be published

(Continued on back cover)

SATELLITE AND MESOMETEOROLOGY RESEARCH PROJECT

Department of the Geophysical Sciences

The University of Chicago

THE SCANNING PRINTER AND ITS APPLICATION TO DETAILED ANALYSIS OF SATELLITE RADIATION DATA

by

Tetsuya Fujita

SMRP

Research Paper #34

July 1964

Research on the Scanning Printer and its construction has been sponsored by the National Science Foundation under NSF G 18984. Basic research on radiation data leading to the development of the analysis techniques presented in this paper was supported by the National Weather Satellite Center, U.S. Weather Bureau under grant CWB WBG - 6 and also by the National Aeronautics and Space Administration under grant NASA NsG 333.

THE SCANNING PRINTER AND ITS APPLICATION TO DETAILED ANALYSIS OF SATELLITE RADIATION DATA

Tetsuya Fujita

Department of the Geophysical Sciences

The University of Chicago

Chicago, Illinois

ABSTRACT

In order to improve the time-consuming analyses of TIROS radiation data for use in mesometeorological studies, a Scanning Printer was designed and constructed. The printer output is a coded printout on a translucent sheet which can be reproduced by a dry diazo process for further analysis of radiation patterns. Because the data are printed out on parallel straight lines which correspond to the curved scan lines on the earth, the patterns contoured directly on the printout sheet are distorted. Nevertheless, the unsmoothed patterns thus obtained give much higher resolution that that expected from FMRT Listings or Grid Print Maps currently available to researchers. This improved printout capability, together with the superimposed grid lines of longitudes, latitudes, solar zenith angles, solar backscattering angles, satellite zenith angles, etc., now permits us to interpret TIROS radiation data in relation to mesoscale disturbances. Moreover, this Scanning Printer can also be utilized in reducing future NIMBUS data. Presented in this paper are the principle and the function of the Scanning Printer and an example of the radiation data analyses which are being carried out at the Satellite and Mesometeorology Research Project, University of Chicago.

1. Introduction

Radiation data transmitted back to the ground stations from TIROS meteorological satellites are processed into meteorologically usable forms. The Final Meteorological Radiation Tapes (FMRT) include the calibrated radiation values and their geographical locations along each scan line on the earth. They are the product of a computer program including the orbital and attitude data, digitized radiation data, and radiometer calibration package. A detailed description of FMRT appears in the TIROS Radiation Data Users' Manuals (1961) (1962) and a Supplement by Bandeen (1962).

Nordberg et al. (1962) published a pioneering work on the analysis of TIROS scanning radiometer data in an attempt to geographically orient and interpret the acquired information. Since then the Grid Print Maps produced by NASA (1961) and (1962) became available to researchers who are interested in studying synoptic scale radiation patterns. When one intends to compare satellite radiation data with ground station data, it becomes necessary to map the radiation patterns in mesoscale. Study of reflected solar energy by using TIROS III and U.S. Station data by Fritz, Krishna Rao, and Weinstein (1964) revealed that such comparison is of extreme value when radiation data are charted in detail.

When we start reducing original analog traces into a form which would permit us to investigate mesoscale atmospheric structures, it is necessary to determine, first of all, the reasonable sampling frequencies which would retain most of the meteorological signals. It is true that the 5^{o} field of view of a scanning radiometer measures a weighted-mean of radiation values within its field of view, thus frequently representing the radiation values from an area much smaller than this field. The radiation data will thus depict objects which are radiatively outstanding but relatively small compared with the half-power field of view. Such examples are seen also in the measurements by radars. We know that a PPI radar of 2^{o} beam width often presents echo structures within this angle, suggesting that the backscattered energy cannot be expressed fully by digitizing the energy at 2^{o} intervals of antenna rotation. Repeated tests indicate that an interval of 2^{o}, or even less, of satellite spin angle is necessary to express in full the meteorological signals recorded on an analog trace. This would suggest a sampling rate of more than 180 points per spin of a TIROS satellite in order to express the energy variation on the trace.

In addition to this field of view, further consideration should be given to the superimposed noise and the frequency response of the instrument itself. To estimate such noise and response, Channels 2 and 3 values read out from analog traces were plotted along a series of scan lines drawn on various photographs. Unless a trace includes obvious noise, cloud and radiation patterns show extremely good coincidence; and it was concluded that about 5 data points within a 10^{o} spin angle of TIROS are required for the depiction of energy variations as a sensor moves over clouds. This result also indicates that a sampling of about 180 points per spin is needed.

The sampling period for early FMRT was set to 72 clock cycles of the satellite clock frequency of 550 cycles per second. This period, 0.1301 sec, would result in about 50 samplings per spin period of the satellite. After TIROS VII, the sampling period was reduced to 36 clock cycles, thus increasing the data points by the factor of two. If we intend to decrease the sampling period further, it becomes necessary to go through a major modification in the FMRT production program. We cannot expect to increase the sampling frequency beyond about 100 per spin period of TIROS at the present time.

In order to overcome difficulties involving more frequent samplings, a system of coding the values on an analog trace through a specially designed encoder was developed. This system which is called the "Scanning Printer" is operated by a driver who follows the trace by turning a steering wheel while adjusting his driving speed to negotiate irregular radiation curves. The values are calibrated, coded, and printed automatically on a sheet of paper by spending about one minute per spin period of the satellite. A prototype Scanning Printer constructed at the University of Chicago samples about 350 data points per spin and is capable of printing at the rate of up to 20 points per second.

The final printout thus produced by the Scanning Printer includes coded radiation values printed along parallel straight lines that represent successive scan lines corresponding to the consecutive spin of the satellite. When the isolines of radiation values are drawn on the printout sheet, it is found that their patterns are distorted from those which are expected to appear on a regular map projection. For geographic identification of these radiation patterns, a geographic grid consisting of longitudes and latitudes needs to be drawn onto the printout sheet.

Despite the fact that the radiation patterns are distorted, it was found that the resolution of mesoscale patterns is much higher than that obtained by other methods. Moreover, an analysis can be performed within a rather short time, thus promising the further application of the Scanning Printer in the detailed mapping of radiation data obtained by satellites.

2. Basic Scan Geometry

Scanning modes of TIROS meteorological satellites were studied by Bandeen (1962) who classified them into closed and open modes of the floor and wall sensors, respectively. The combination of these modes and sensors results in three basic scanning modes: closed mode, single open mode, and alternating open mode. When the satellite height increases beyond a critical value, there appear periods when the earth is not scanned at all by either sensor;Fujita (1964) called this mode the null mode. This mode, however, does not appear in the case of current TIROS satellites.

Now we shall consider a sensor with the inclination of radiometer axis (β) measured from the scan axis around which the radiometer axis rotates. For TIROS radiometers the scan axis is identical to the vehicle's spin axis, and the sensor axes extending toward the floor and the wall of a satellite are identified as floor and wall sensors, respectively. As a spin-stabilized satellite orbits around the earth, the nadir angle of the scan axis, or the scan-axis nadir angle (η_a), varies between maximum and minimum values. When this minimum value, which is the minimum nadir angle (η_o) for TIROS, is zero, the spin axis is included within the plane of the orbit. Defined in Fig. 1 are the subpoints at which the first scan (FS), the first closed mode (FC), the minimum nadir angle (AX), the last closed mode (LC), and the last scan (LS) of a specific sensor take place.

The scan-axis nadir angles for these subpoints are expressed by

$$\eta_a^{FC} = \eta_a^{LC} = 90 - \beta - \delta_H \ , \qquad (1)$$

$$\eta_a^{FS} = \eta_a^{LS} = 90 + \beta - \delta_H \ , \qquad (2)$$

and $$\eta_a^{AX} = \eta_o \ , \qquad (3)$$

where δ_H denotes the dip viewed from the satellite height. The designator AX represents the axial point, a subsatellite point in each orbit at which the minimum nadir angle takes place. When the minimum nadir angle is not zero, AX in Fig. 1 may be altered into the spin-axis point (SA) so that the geocentric angle between AX and any subpoint represents the scan-axis nadir angle or the satellite nadir angle (η_s) for TIROS.

The terrestrial scan lines, loci of the scan points on the earth, are located inside a closed area elongated along the subpoint track. In order to avoid complications in scan geometry, we first consider the case of a non-rotating earth, thus forming fixed-earth coordinates as introduced by Fujita (1963). When the minimum nadir angle is zero, the spin-axis point and the axial point coincide, resulting in a symmetric scan area with respect to the fixed-earth subpoint (FSP) track. As illustrated in Fig. 2, the positions of the first scan and the first closed-mode subpoints are obtained on the FSP track from Eq. (1) and (2).

If the minimum nadir angle is not zero, the geocentric angle between FS and AX measured along the FSP track is expressed by

$$\begin{aligned} \cos \theta^{FS} &= \sec \eta_o \ \cos \eta_a^{FS} \\ &= -\sec \eta_o \ \sin (\beta - \delta_H) \ , \end{aligned} \qquad (4)$$

and that between FC and AX, by

$$\begin{aligned} \cos \theta^{FC} &= \sec \eta_o \ \cos \eta_a^{FS} \\ &= \sec \eta_o \ \sin (\beta + \delta_H) \ . \end{aligned} \qquad (5)$$

These equations indicate that the earth is not scanned at the axial point when

$$-\sec \eta_o \sin(\beta - \delta_H) > 1$$

or

$$\eta_o > 90° + \beta - \delta_H \ , \qquad (6)$$

and that no closed mode scanning takes place at the axial point when

$$\sec \eta_o \sin(\beta + \delta_H) > 1$$

or

$$\eta_o > 90° - \beta - \delta_H \ . \qquad (7)$$

For TIROS radiometers with $\beta = 45^o$ and its height with dip, $\delta_H \cong 27^o$, the earth is always scanned at the axial point, since $90^o + \beta - \delta_H \cong 118^o$ is greater than 90^o, which is the upper limit of the minimum nadir angle. If the minimum nadir angle is greater than $90^o - \beta - \delta_H \cong 18^o$, however, there occurs no closed-mode scanning throughout the entire orbit.

Figure 2 also shows schematically the scan areas which vary appreciably with an increasing minimum nadir angle from zero to about 30^o. The left half of the figure includes the scan lines and the primary lines when the satellite is located at the first scan and first closed-mode subpoints; and the right half, the instantaneous scan lines obtained by rotating the scan axis instantaneously at the successive positions of the satellite.

It is seen that the scan area is enclosed by four lines which are (A) the First Horizon Track, a locus of the scan points at the apparent horizon at which the radiometer axis intersects the earth as it moves from space to earth, (B) the Second Horizon Track, a locus of the scan points at which the sensor axis leaves the earth toward space, (C) the Inner Scan Boundary, an envelope to a group of scan lines which is closer to the spin-axis point than the other envelope if it exists, and (D) the Outer Scan Boundary, the other envelope which exists only when closed mode scanning takes place.

It is of importance to find that the scan lines within a scan area of a specific sensor often intersect each other. The area which includes such intersections is obviously characterized by dual radiation values which are usually measured from different directions with different zenith angles. For mesoscale analysis of radiation

data, it is the usual practice to map these values on two separate charts, the initial scan chart and the complemental scan chart. These charts include, respectively, a group of non-intersecting scan lines that begins at the first scan perinadir, and the other group that ends at the last scan perinadir. The perinadir is the scan point having the smallest nadir angle of view of all scan points on an instantaneous scan line.

The spin-axis point of the wall sensor is identical, at any moment, to the spin-axis antipode of the corresponding floor sensor. On the fixed-earth coordinates, the scan area of one sensor can be obtained by shifting the whole area exactly 180° along the FSP track and by forming a mirror image with respect to this track. In many cases, the complemental scan lines of one sensor intersect the initial scan lines of the other, thus permitting us to construct dual radiation charts over the same area. Such an overlapping in scan areas is shown in Fig. 3. Note that the initial scan lines include the first scan perinadir where the scan cone of a specific sensor first makes contact with the earth; and the complemental scan lines, the last scan perinadir.

3. Scan Angle vs. Time Coordinates

A medium-resolution radiometer on board a TIROS satellite continuously scans either space or the earth, thus its angle of scan increases in proportion to the time passage. By completing about 10 scans per min, the sensor axis rotates 3600° per min, $216,000^{\circ}$ per hour, or over five million degrees per day. Only the radiation values during the past 100 min are stored on an endless tape on board the satellite and read out during each pass over the proper readout stations. The data are later recorded in the form of analog traces so that they can be reduced and analyzed for research purposes. Figure 4 shows an example of these analog traces, including five-channel radiation values and sun and TV pulses at the bottom.

If we assume that the recording and playback speeds of the satellite-borne tape-recorder as well as the recording rate of the analog traces are constant, the length of the analog trace (L) is proportional to the accumulative scan angle (θ) of a sensor or the spin angle of a TIROS. We may thus write

$$L = c\theta \qquad (8)$$

where c designates the recording rate.

The trace length between two consecutive sun-pulses corresponds with a high degree of accuracy to one complete scanning with respect to fixed-space. This trace length may be considered constant, at least within one orbital period, and called the fixed-space scan length (ΔL_s). We may thus count the fixed-space scan number by dividing an analog trace into sections between consecutive sun-pulses which appear except when a satellite moves inside the earth's umbra.

The terrestrial scan length (ΔL) is defined as the length on an analog trace between two consecutive aponadirs which are located at the center of the space-viewing trace by a specific sensor. This length is not constant because the primary plane, which always includes an aponadir, rotates due to the orbital motion of the satellite (see Fig. 5). The rotation angle of the primary plane or line can be measured at the satellite in the plane perpendicular to the TIROS spin axis. This plane is parallel to a plane which is tangent to the earth at the spin-axis point. As shown in the figure, therefore, the direction of the primary line can be expressed by the spin angle of the primary line (μ^{PM}) measured from a spin-angle reference in fixed-space. We may express the terrestrial scan length of j scan number, thus

$$\Delta L_j = \Delta L_s + \frac{\partial \mu^{PM}}{\partial t} c \, \Delta t_j \quad , \qquad (9)$$

where Δt_j is the terrestrial scan period, the period between two consecutive aponadirs.

Now we divide an analog trace into a constant scan length ΔL_s and number each scan length 0, 1, 2 . . . . . , which are the fixed-space scan numbers. If we plot radiation data from these scan lengths along a group of data lines in Fig. 6, the horizontal distance (p) of these data lines represents the fixed-space scan period (Δt_s). It is evident that the slower the scan rate, the larger the tilt of the data lines. The time lines, considered as instantaneous scan lines, are obtained by connecting the upper end of each data line with the beginning of the next data line. The ordinate represents a magnified scan length (m ΔL_s) which corresponds to 360^o scan angle of the sensor.

Sigma-t Chart. The abscissa of the above-mentioned coordinates is proportional to time and the ordinate, to the scan angle (σ) of the sensor. A chart with radiation data on such coordinates is called, therefore, a sigma-t chart.

Equation (9) indicates that the position of the aponadir on each data line changes gradually as a result of the accumulative angles given by the second term on the right side. The terrestrial scan lengths and their numbers can thus be obtained on a sigma-t chart by finding the intersections between the aponadir line and the data lines. Note that the fixed-space scan numbers deviate gradually from the terrestrial scan numbers. Since the primary line rotates 360^{o} during one orbit, these scan numbers differ by one, either plus or minus, at the end of each nodal period.

In view of the fact that the earth-scanning period is much greater along the perinadir line on the sigma-t chart than along the aponadir line, the former ($\sigma = 180^{o}$) is usually determined on a sigma-t chart by dividing the distance between the first and second horizons into two equal parts.

The Scanning Printer designed by the author is capable of printing automatically the radiation data directly from an analog trace while an operator follows the line on the trace.

4. Scanning Printer

There are several scanners available on the market, but they are designed to stop the cross-hairs at a desired position in order to digitize x and y coordinates by pressing a button. It usually takes about 10 seconds to read out one data point, thus requiring 10 to 20 minutes per complete scan of a specific sensor. These digitized data are put into a computer for calibration before plotting them on a chart of a desired projection. During 1962 and 1963 several cases were analyzed by using an available scanner with which hours were spent to reduce radiation data over a relatively small area.

To overcome such time-consuming efforts required for the utilization of analog traces, a prototype Scanning Printer was constructed in 1963. As shown schematically in Fig. 7, it is designed to follow manually a curve on an analog trace with cross-hairs.

The displacement of the vertical hair is fed into an encoder of a printed circuit board which calibrates the values on the analog trace into desirable units before the signals are transmitted into a traveling printer with eight print arms.

The printer, driven by a printer shift thread with pitch p, translates rightward by the distance p while the analog trace travels beneath the cross-hairs by the trace length corresponding to ΔL_s in Eq. (9). It is evident that the radiation data printed on a sheet of paper wrapped around the printing drum represents values on a sigma-t printout chart as presented in Fig. 6.

An entire view of the prototype printer, completed early in 1964, appears in Fig. 8. The mechanism to the left for following the analog trace is rigidly connected with gears to the printing mechanism to the right. The main-drive motor (see Fig. 9), a 60-watt sewing machine motor with a speed control foot-switch drives the main wheel at a variable speed of a few to 20 rpm. During each revolution, two pulse contacts make simultaneous contact with a pulse ring, thus creating a positive pulse which activates a D.C. relay to generate an A.C. pulse which activates the printer solenoids. Since the pulse ring extends within a 165° tangential angle of the main wheel, the pulse length is inversely proportional to the revolution rate of the main wheel. To avoid a prolonged positive pulse, which creates heat and noise in the printer solenoid, an escape mechanism is added next to the pulse contact. This mechanism allows the main-drive motor to keep turning at a rather slow rate as long as the pulse contacts are on the pulse ring, thus avoiding the occurrence of an extended activation of the solenoid.

The revolution of the main wheel is transmitted to the worm gear connection in Fig. 10. Then the revolution of this worm gear is transmitted without reduction to the printer drum through a frictional coupling gear system which can be engaged or disengaged by an operator using a coupling lever. Thus the angular velocity of the worm gear is transmitted to the printer drum as long as the coupling lever is in "engage" position. The revolution rate of the worm gear is reduced to 1 : 5 by reduction gears before it is transmitted to the analog trace drum. The ratio of the linear speeds at the surfaces of the analog trace drum (3.5" dia) and the printer drum (5.5" dia) is, therefore, 1 : 7.86, which would magnify a length of 56 mm or an analog trace into 439 mm, the circumference of the printer drum. When an analog trace is recorded at

the rate of 40 cm per min of the satellite time, 10 rpm of the vehicle's spin results in a 400-mm trace length per fixed-space scan of the radiometer. As a result, the printout data corresponding to a fixed-space scan are always shorter than the circumference of the printer drum, thus necessitating the manual rotation of the printer drum until the printing arms are reset at the start line for the following fixed-space scan.

Figure 11 shows a print-length selector which is adjusted by an operator so that the machine automatically stops as soon as the printout reaches a preset length. The print length varies according mainly to the spin rate of the satellite and also to the recording and to the playback speed of the satellite-borne tape-recorder, and also to the recording rate of the analog trace made on the ground. The printer, which is shifted slowly by a printer shift thread, consists of eight 110-volt solenoids which pull up the printer arms connected to eight printing heads placed on a 4-mm segment of a straight line parallel to the printer-drum axis. As these printing heads strike a sheet of paper wrapped around the printer drum, a printer ribbon traveling between the printing head and the paper produces clear print marks on the paper. The printer shift thread is rotated by a pitch adjuster which is connected by a rubber belt to a pulley at the end of the printer drum. The pitch adjuster is designed to adjust the ratio of the rotation of the printer drum and the printer-shift thread so as to leave a desirable space between the data lines.

The signals to operate the printer solenoids are generated by an encoder system (see Fig. 12), consisting of a calibration board made of a printed circuit contact surface and eight pieces of wipers designed to be moved in left-right directions by a driving wheel which is hooked onto the vertical lines to which the cross-hairs are attached. For design of this encoder, Bohan's (1962) idea of coding radiosonde data for graphical representation is used. His codes or notations are designed to print out a series of upper-air temperatures into narrow bands of upright areas so that the variation in temperature along the vertical can easily be evaluated. A schematical diagram of the notations used in this scanning printer is presented in Fig. 13. Seen to the left in an upright position is a printed circuit board with metallic contacts in black. A wiper system slides up and down on this board while the operator follows the analog trace by turning a steering wheel. The contacts made to encode the calibrated

vertical scale activate the individual solenoids as each wiper slides over them. The final printout, as it appears at the bottom of the figure, is made within a belt 4 mm wide and up to 439 mm long, the circumference of the printer drum. While printing this length, the 1 : 100 worm-gear ratio and the 1 : 5 ratio of the diameters of the main wheel and the worm-shaft pulley (see Fig. 9), 500 pulses are generated, thus producing dots or lines at 0.88-mm intervals which remain the same regardless of the trace-scanning speed selected by the operator.

If the spin rate of a satellite is N rpm, the analog-trace length per scan is one Nth of 400 mm. Knowing that 500 points are printed out per 56-mm length of the analog trace, we obtain the number of printout points per scan, thus

$$\frac{400}{N} \times \frac{500}{56} = \frac{3570}{N} \quad .$$

In other words the scanner prints out an average of about 350 points per scan. An experienced operator can follow a scan length of an analog trace in 30 to 60 sec in which period 5 to 10 pulses per min are generated to activate each solenoid.

5. Geographic Grids and Isolines on Sigma-t Charts

A large number of sigma-t printout charts have been produced in an attempt to analyze them for mesometeorological interpretation of TIROS radiation data. For geographic identification purposes, however, each printout chart should be transferred onto a proper map projection, or a group of longitude and latitude lines should be superimposed on the printout chart. A series of tests revealed that it is convenient to interpret radiation patterns on the printout chart by simply distorting geographic grids so that they fit exactly to the original printout.

Presented in Fig. 14 is an example of radiation data printed out by using the Scanning Printer. The printout was made from TIROS III R/O Orbit 289 between 1253Z and 1302Z, August 1, 1964 when the satellite moved from western Brazil to the south Atlantic Ocean. The satellite nadir angle, which is identical to the scan-axis nadir

angle, was decreasing from about 60^{o} to 34^{o} during this printout period, thus increasing the earth-scanning period in each scan. Note that the distance between the first horizon at the bottom and the second horizon at the top increases toward the right.

During this period a series of tape-mode pictures was taken at 30-sec intervals. Three frames gridded by a 7094 computer at the University of Chicago are shown in Figs. 15 through 17. The accuracy of the grid lines on these pictures is better than 0.2^{o} geocentric angle, since they were obtained by the computer on a distortion-free picture coordinate and then hand-transferred onto the distorted picture, taking both lens and electronic distortions into consideration.

In order to correlate the cloud patterns on these pictures with radiation patterns, one first determines the longitude and latitude lines distorted to fit the sigma-t printout chart (see Fig. 18) and then transfers the cloud patterns in the pictures to the sigma-t coordinates (see Fig. 19). By doing so, the printout sheet can be examined and also contoured by superimposing a short-wave radiation printout onto these transferred cloud patterns. The numbers 1, 2, 3, ..., designating significant features on the pictures, are transferred onto Fig. 19 so as to investigate the radiation values associated with these features. These numbers are also included in Fig. 20 which represents Channel 3 ($0.3 - 4\mu$) radiation patterns contoured carefully on a sigma-t printout chart.

Similar radiation charts can be obtained for other radiation channels within a short time. The window channel (Channel 2) analysis is shown in Fig. 21 in order to compare the brightness patterns with those of temperatures averaged over the radiometer's field of view.

When we compare the cloud distribution on gridded photographs, with the patterns of reflected light on a Channel 3 chart, and also with the window-channel radiation patterns, all of which are analyzed independently, it will be found that the features on these three charts correspond extremely well. Relatively small but dark areas, 15, 16, 17, and 23 in Fig. 15, for instance, appear on Channel 3 chart as narrow low reflectance areas and on Channel 2 chart as distinct warm areas. Relatively bright areas, 38, 39, 49, and 51 in Fig. 16, are clearly identified as the domes of high reflectance areas on Channel 3 chart and as relatively cold areas on Channel 2 chart. Of interest are areas

9 and 10 in Fig. 15 which are not bright at all on the Channel 3 chart, nor in the photograph. At least 10 scans over these areas equally indicate a reduction of effective radiant emittance, some from 40 to 33 watts m^{-2} corresponding to 268K to 257K or about 10C reduction in equivalent blackbody temperature. These areas are characterized by probably thin cirrus or cirrostratus cover.

If one prefers, the radiation patterns on sigma-t printout charts can be transcribed onto other charts of any projection or onto cloud pictures. Figure 22 is an example of the isolines of Channel 3 data in watts m^{-2} drawn on Frame 11, R/O 289, TIROS III. The radiation contours do not represent fine structure of cellular clouds; nevertheless, they show a general increase in reflectance over the areas of densely populated cells. Near the northwest horizon the countours are characterized by a tight gradient, suggesting the existence of activities in lines. There is only one location in the picture at 29S and 45W where reflectance is zero. The picture indicates that there were no clouds when scanning took place.

In order to further interpret short-wave radiation data, it is necessary to draw on a sigma-t chart the isolines of the solar zenith angles (ζ^*) and the backscattering angles (ψ_b), which are 180° less than the scattering angles (Fig. 23). From these isolines both angles can be interpolated immediately at any given points on the sigma-t chart. The solar zenith angles are used in computing reflectance:

$$R = \frac{\overline{W}}{\overline{W}^* \cos \zeta^*} ,$$

where $\overline{W}$ denotes the effective radiant emittance and $\overline{W}^*$, the effective solar constant defined by

$$\overline{W}^* = \frac{\Omega}{\pi} \int_0^\infty W \, \phi_\lambda \, d\lambda ,$$

where Ω is the solid angle of the sun viewed from the scan point, W, the solar radiant emittance, and ϕ_λ , the spectral response of the short-wave radiometer. The backscattering angle is also important, since the scattered light from clouds within the field

of view is far from isotropic. We still do not know this directional characteristic; however, it seems that there are two maxima in the directions $\psi_b = 0^o$ and $\psi_b = 180^o$, which are restricted for radiation measurements because one of the sensors includes the direct radiation from the sun. If we avoid these extreme backscattering angles, it is feasible to determine the directional characteristics of scattering by analyzing initial and complemental radiation data on sigma-t printout charts.

For better interpretation of long-wave radiation characterized by significant limb darkening, determination of the zenith angle of the satellite (ζ^{SAT}) viewed from a scan point is useful. Using this zenith angle (see Fig. 24) and known limb-darkening values such as obtained by Wark, Yamamoto and Lienesch (1962), we can calculate effective radiant emittance measured while hypothetically viewing straight down. The zenith angle of the satellite, when combined with the satellite height, permits us to compute the dimensions of scan spots on the earth.

6. Conclusions

A Scanning Printer designed by the author permits us to print out unsmoothed and calibrated radiation data while simply following an analog trace of a desired channel. By printing out at the average rate of 10 points per sec and 350 points per complete scan of a radiometer axis, an operator can produce a sigma-t printout chart covering 10-min data within a couple of hours. Since the printout notations are capable of pictorially representing the gradient as well as the absolute value, the isolines of unsmoothed contours can be drawn quickly and accurately. The radiation patterns thus obtained designate the detailed radiative structure of terrestrial objects and thus make it possible to carry out mesoscale investigation of cloud distribution not otherwise feasible.

A large number of graphs and nomographs, in addition to 7094 computer outputs, now enable us to analyze radiation data as well as cloud pictures from any TIROS within a very short time with an accuracy better than 0.2^o geocentric angle. A graduate student, for instance, can perform basic radiation and cloud mapping over an area comparable to that of the United States within two weeks. Since the printout data are

unsmoothed, the final results are comparable to a so-called mesosynoptic analysis of satellite data which can be compared with other data such as radar echoes, mesoscale surface charts, etc.

The sigma-t chart never mixes the initial and complemental scan data either in open or closed-mode scanning cases. The analysis of these data is performed separately on a printout chart so that the dual measurements of the same area can be compared afterwards. First, the limb-darkening phenomena are studied by selecting data pairs within the same area measured from two different zenith angles of the satellite. Second, the reflectance of an area is measured from two different backscattering angles appearing in complemental and initial scan areas. Accumulation of such analyses will permit us to establish un-isotropic characteristics of scattering by terrestrial objects.

Acknowledgements:

The author is very grateful to Mr. Vincent Ankus for his efforts in constructing a prototype Scanning Printer after repeated modification of both the mechanical and electrical systems which successfully printed out over 7 million prints after their completion. Sincere gratitude should be expressed to other staff members of SMRP (Satellite and Mesometeorology Research Project) who rendered assistance in completing this research.

Research on the Scanning Printer and its construction has been sponsored by the National Science Foundation under NSF G 18984. Basic research on radiation data leading to the development of the analysis techniques presented in this paper was supported by the National Weather Satellite Center, U.S. Weather Bureau under grant CWB WBG - 6 and also by the National Aeronautics and Space Administration under grant NASA NsG 333.

REFERENCES

Bandeen, W. R., 1962: TIROS II radiation data user's manual - supplement. NASA, Goddard Space Flight Center, Greenbelt, Md., 13 pp.

Bohan, Walter A., 1962: A numeric-pictorial display for meteorological observational data. J. appl. Meteor., 1, 333-342.

Fritz, S., P. Krishna Rao, and M. Weinstein, 1964: Satellite measurements of reflected solar energy and the energy received at the ground. J. atmos. Sci., 21, 144-151.

Fujita, T., 1963: A technique for precise analysis of satellite data; Vol. I - photogrammetry. Meteorological Satellite Laboratory Report No. 14, U.S. Weather Bureau, 104 pp.

Fujita, T., 1964: A technique for precise analysis of satellite radiation data; Vol. II - radiation analysis, Section 6. SMRP Res. Paper 29, Univ. of Chicago, 107-126.

NASA, 1961 and 1962: TIROS II and III Radiation Data Catalogs. Staff Members of Goddard Space Flight Center, Greenbelt, Md., 356 pp and 388 pp.

NASA, 1961 and 1962: TIROS II and III radiation data user's manuals. Goddard Space Flight Center, Greenbelt, Md., 71 pp.

Nordberg, W., W. R. Bandeen, B. J. Conrath, V. Kunde, and I. Persano, 1962: Preliminary results of radiation measurements from the TIROS III meteorological satellite. J. atmos. Sci., 19, 20-29.

Wark, D. Q., G. Yamamoto, and J. H. Lienesch, 1962: Methods of estimating infrared flux and surface temperature from meteorological satellites. J. atmos. Sci., 369-384.

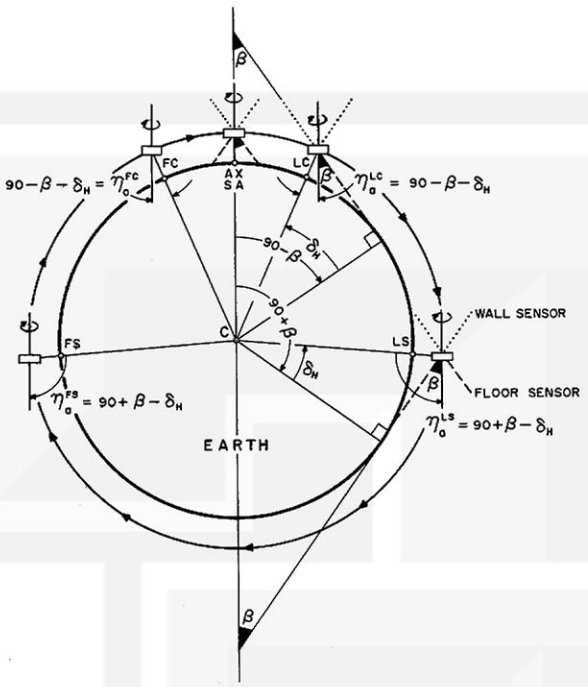

Fig. 1. Changes in the scanning modes of a specific sensor as a satellite orbits around the earth. The figure illustrates the case of zero minimum nadir angle; however, it is applicable to general cases simply by changing the axial point into the spin-axis point. Abbreviations: First Scan Subpoint (FS), First Closed Mode Subpoint (FC), Axial Point (AX), Spin-axis Point (SA), Last Closed Mode Subpoint (LC), Last Scan Subpoint (LS), Inclination of Radiometer Axis (β), and Scan-axis Nadir Angle (η_a).

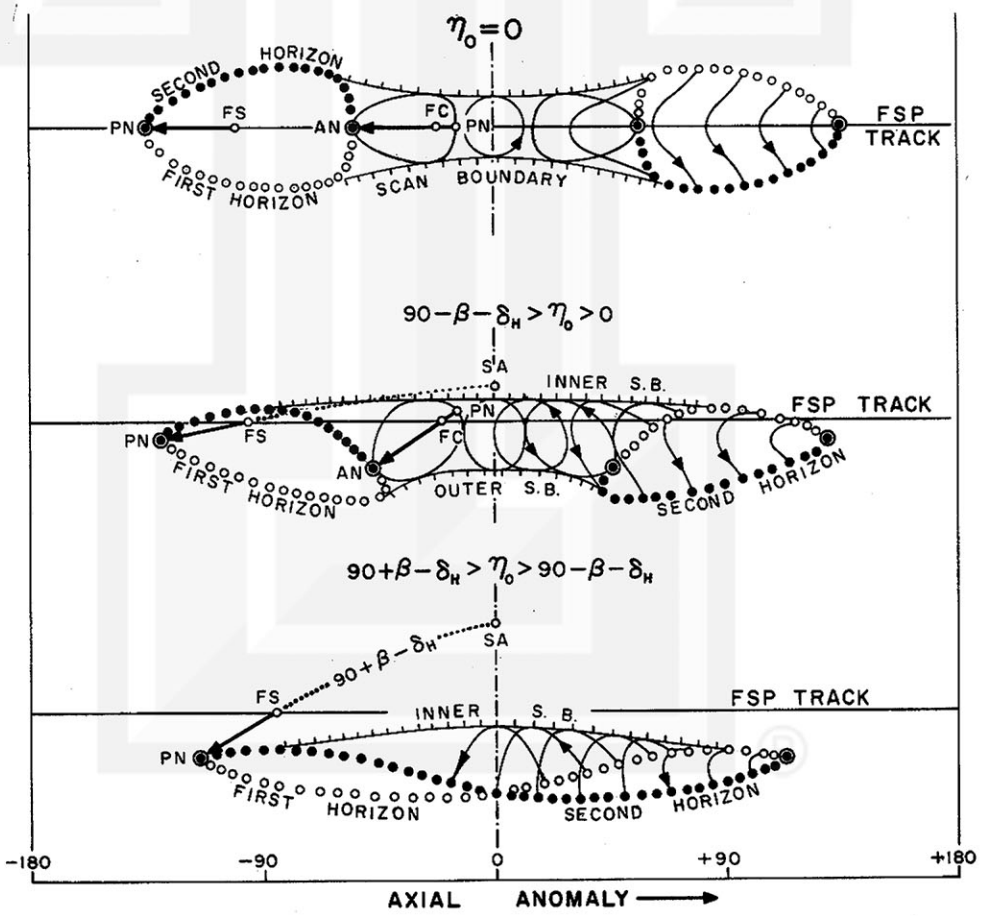

Fig. 2. Three basic scan patterns of a specific sensor. Top: case of zero minimum nadir angle which produces symmetric fixed-earth scan lines with respect to the FSP track. Middle: area including the closed mode scanning, commonly seen in TIROS scan areas when the minimum nadir angle is less than $90-\beta-\delta_H$, which is about 18° for conventional TIROS. Bottom: scan areas without including closed mode scanning. No outer scan boundary appears in this case and the scan area is enclosed by the first and second horizon tracks and the inner scan boundary.

Fig. 3. Combined scan areas produced by floor and wall sensors. In order to avoid mapping the overlapping radiation data it is often necessary to separate scan lines into initial and complemental scan lines consisting of non-intersecting groups of scan lines by a specific sensor as shown in the middle and bottom diagrams of the figure. The initial scan area starts from the point where the axis of a scanning radiometer first makes contact with the earth; this point is called the first scan perinadir.

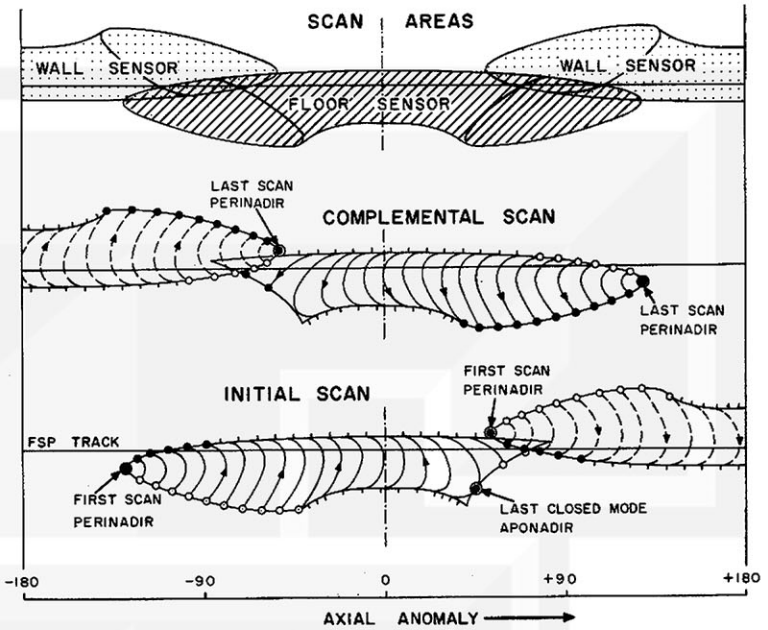

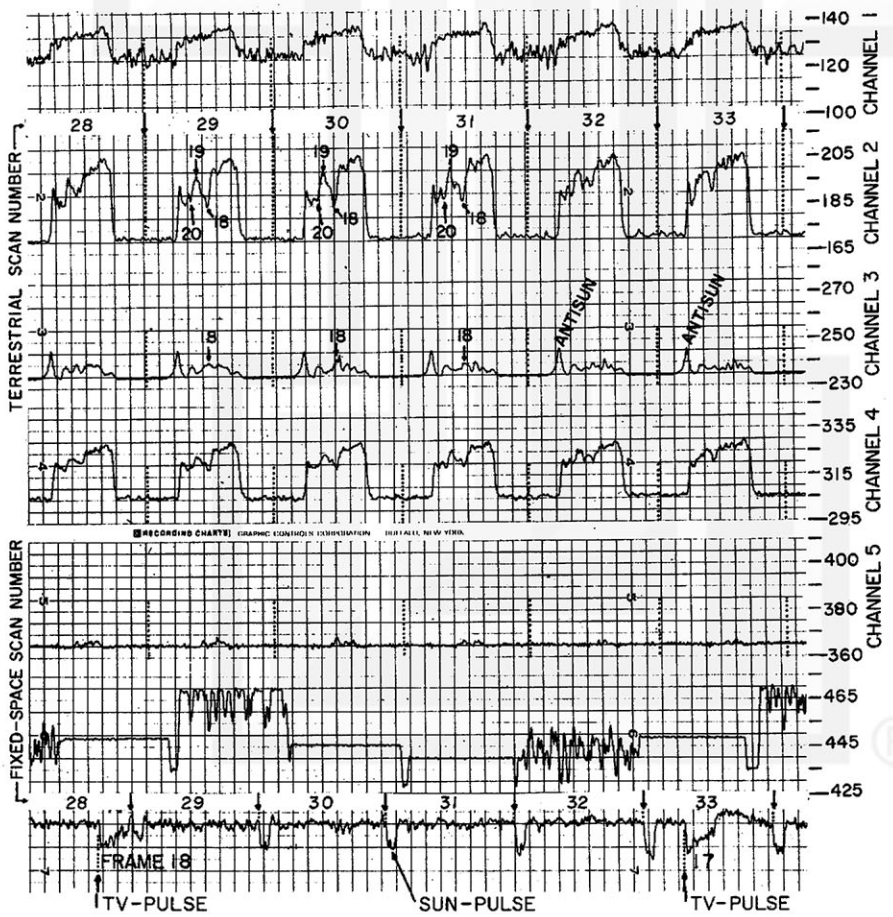

Fig. 4. A portion of the analog trace from TIROS III Orbit 288 which was used in this paper. Vertical dotted lines indicate aponadir for each scan. Recorded at the bottom are TV- and sun-pulses. Note that the frame number of the tape-mode picture increases right to left. The significant point numbers 18, 19, and 20 on Channels 2 and 3 traces designate the same points given in Figs. 20 and 21.

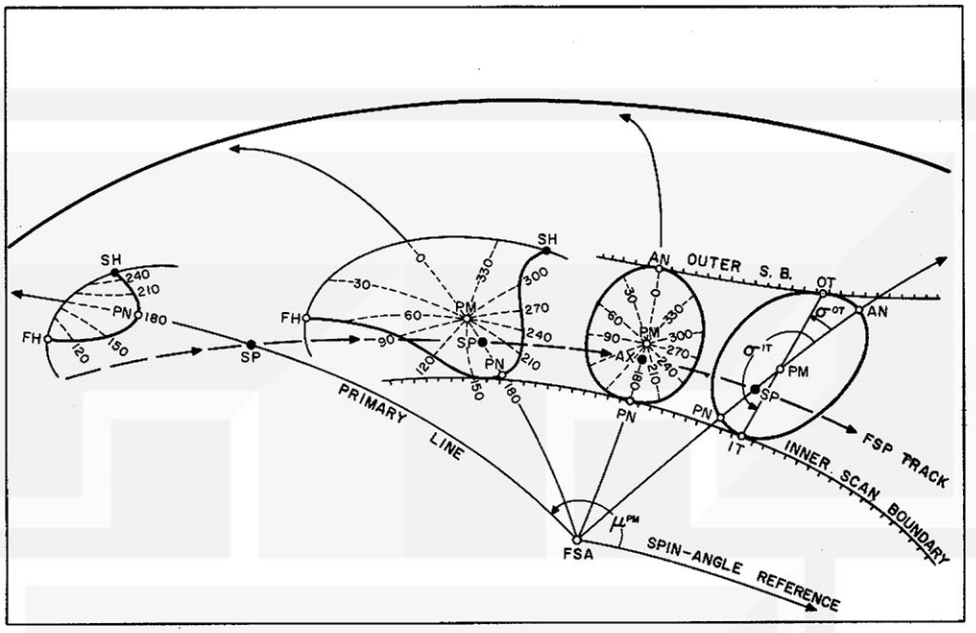

Fig. 5. Scan lines on the earth produced by a sensor as the scanning mode changes from open to closed mode. Broken lines radiating from the primary point (PM) are those of scan angles that are 0° at the aponadir (AN) and 180° at the perinadir (PN). The figure was made on fixed-earth coordinates while scanning the earth instantaneously at each position of the satellite, thus avoiding the appearance of helical scan lines in closed-mode scanning. Beside AN and PN, the points where the scan boundaries meet the scan line tangentially are important in data analysis. They are called the inner tangent point (IT) and outer tangent point (OT).

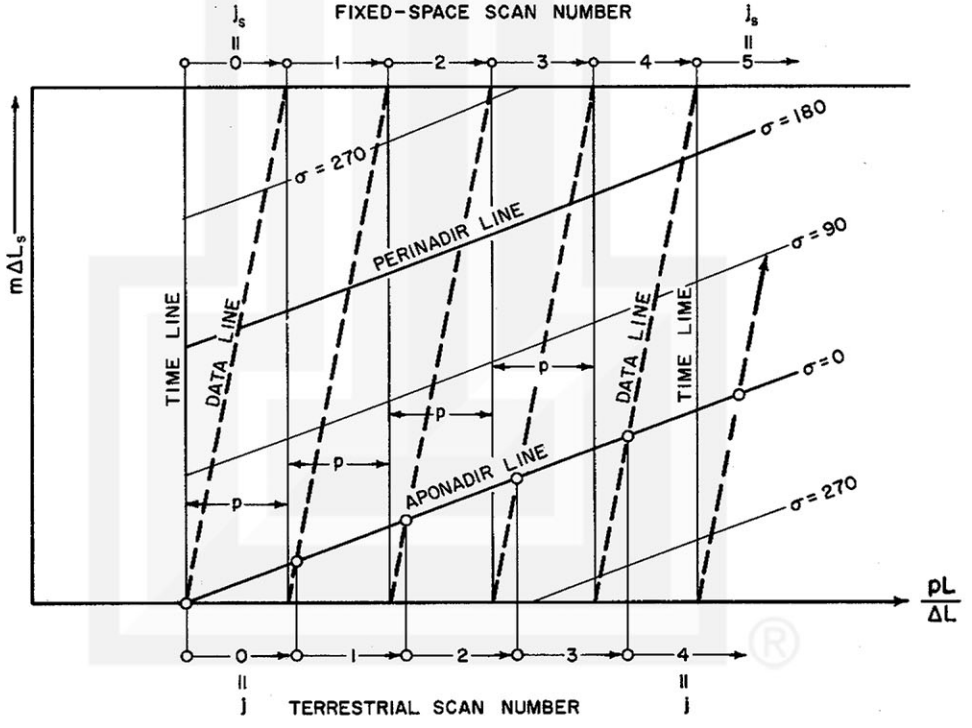

Fig. 6. Schematic diagram of a sigma-t Chart. The time lines on the charts are parallel vertical lines connecting the upper ends and the beginning of successive data lines which are slanted and separated by p, the pitch. Along each time line the scan angle changes 360°. The fixed-space number, which is the count of data lines on the chart, is slightly different from the earth scan number. On the analog trace each earth scan is clearly distinguishable whenever open-mode scanning takes place, and can be numbered.

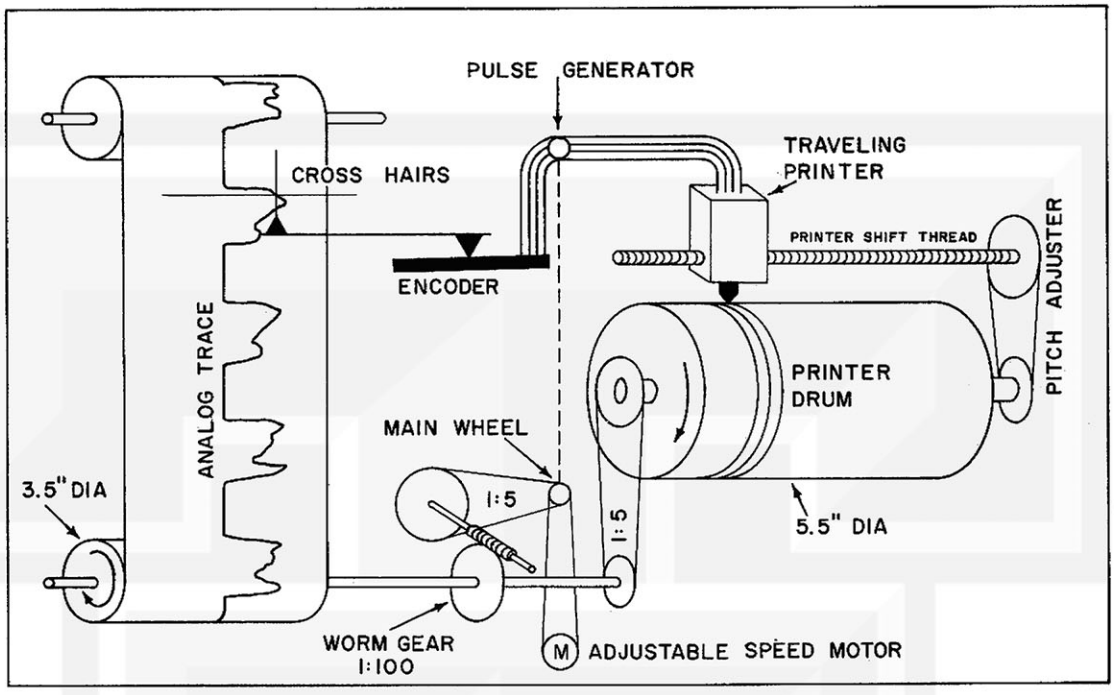

Fig. 7. Schematic diagram of a prototype scanning printer capable of printing out the coded and calibrated radiation values up to 20 points per sec. About 350 points per complete scan length of an analog trace are printed out on a sheet of paper around the printer drum while an operator follows the analog trace with cross-hairs.

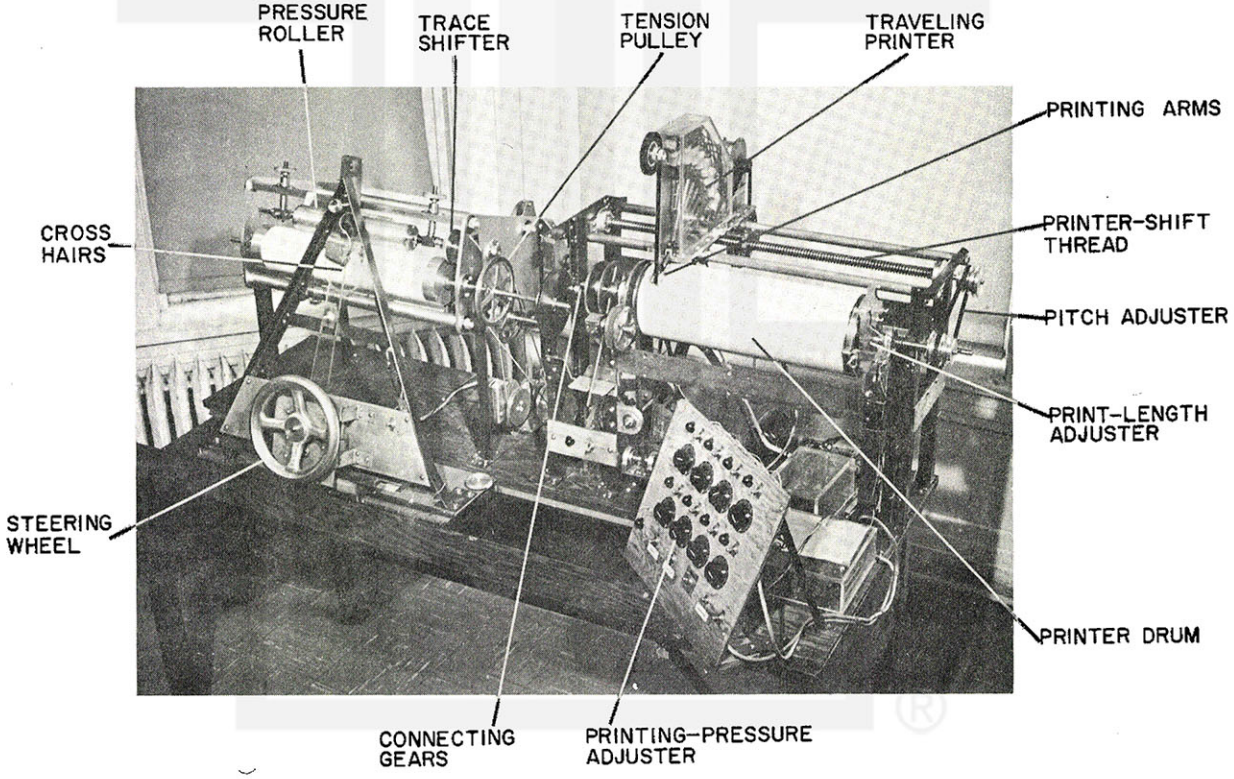

Fig. 8. A view of the Scanning Printer assembled for operation. Trace-following mechanism to the left and the printing mechanism are connected mechanically and electrically with gears, wires, and relays. The darkness of the individual printout points can be adjusted by eight dials, the printing pressure adjusters.

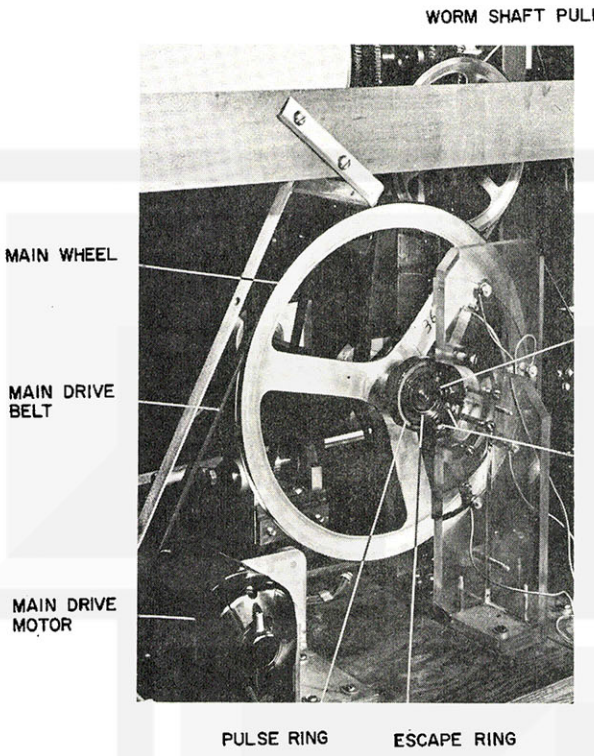

Fig. 9. Close-up view of a pulse generator mechanism located at the back of the Scanning Printer. The main wheel to which the mechanism is attached is driven by a variable speed main-drive motor at lower left.

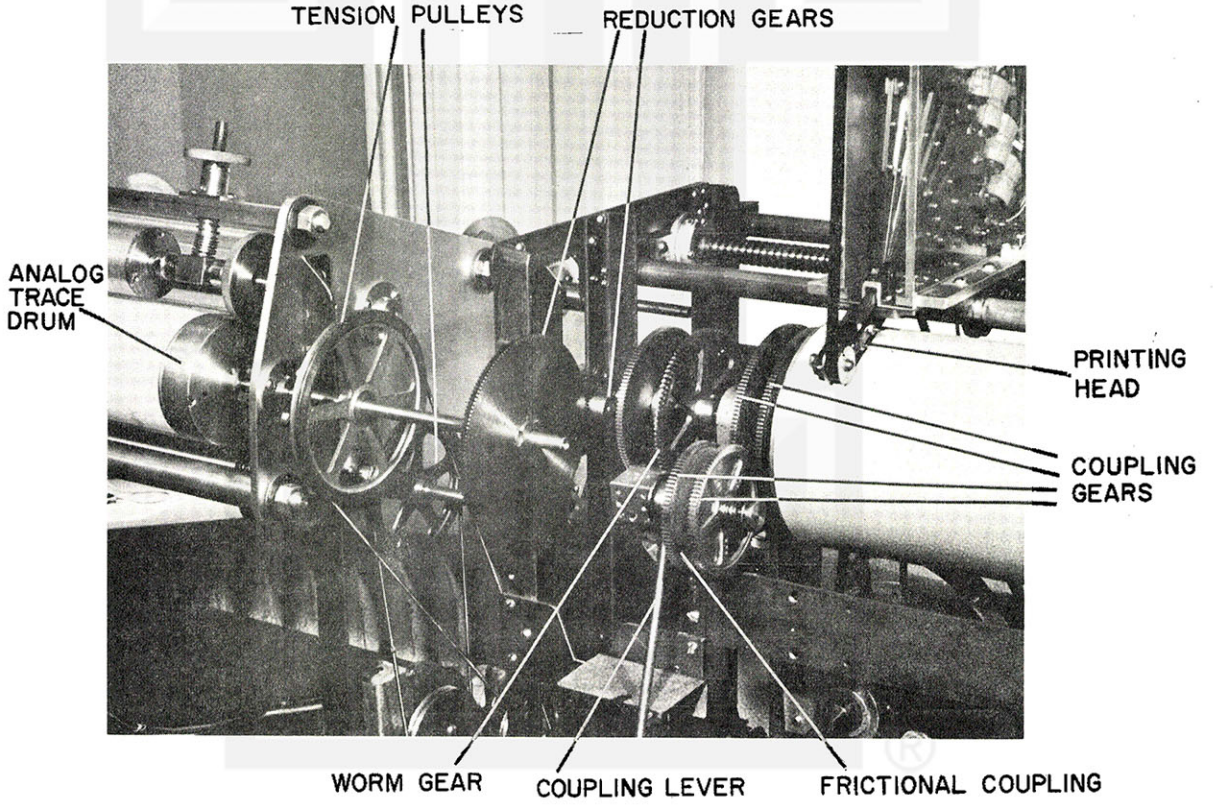

Fig. 10. Gear connection between the analog trace drum and the printer drum. The power transmission from the worm gear to the printer drum can be interrupted by moving a coupling lever each time at the end of each scanning.

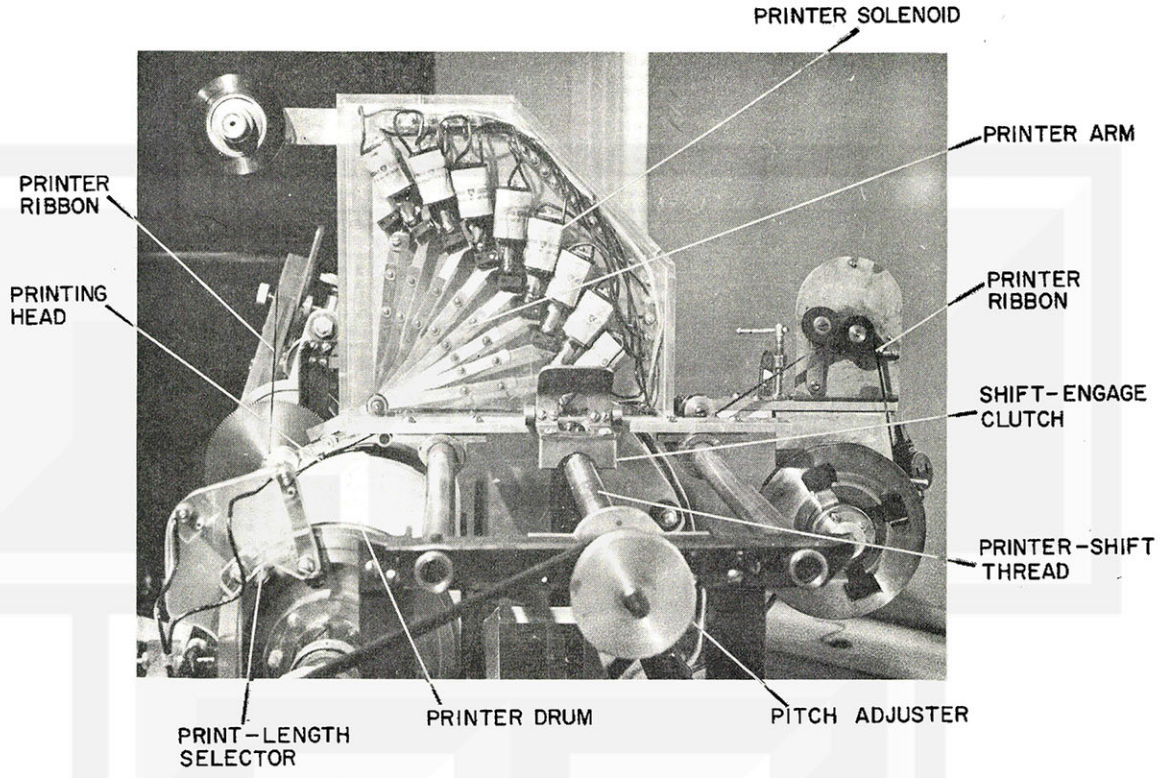

Fig. 11. Side view of the Printer mechanism. Kept in a plastic box to reduce the noise level are eight solenoids and printer arms made of brass which prevent the arms from sticking to the solenoid plunger due to magnetization.

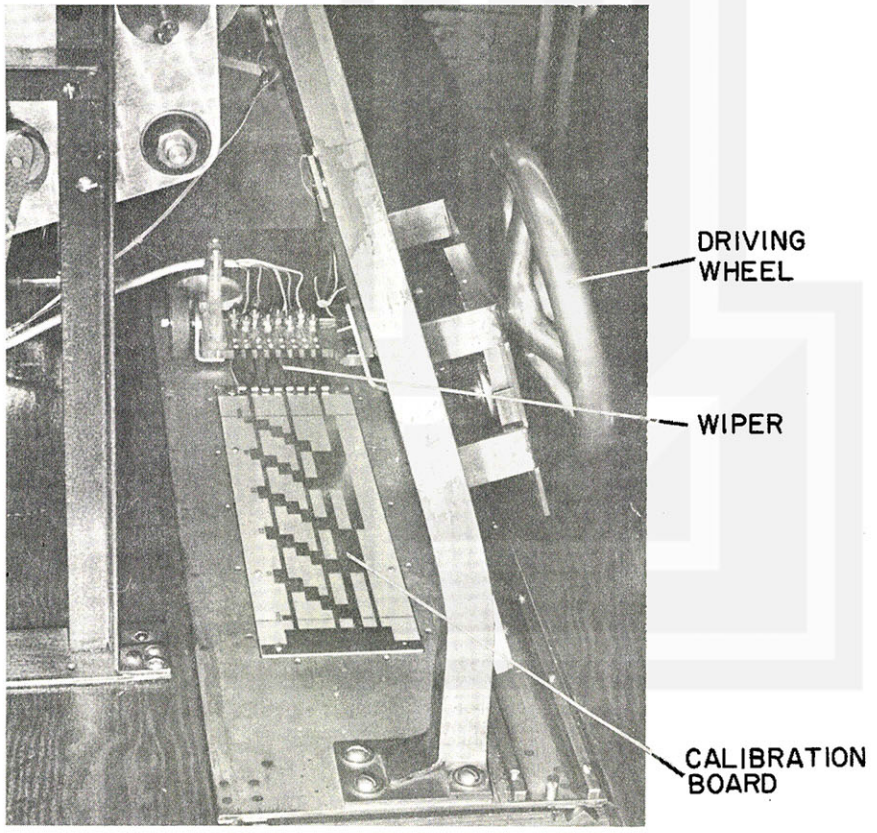

Fig. 12. Encoder and driving wheel assembly. Eight pieces of wiper contacts slide on a calibration board with metallic contacts made to convert calibrated values into coded electric signals.

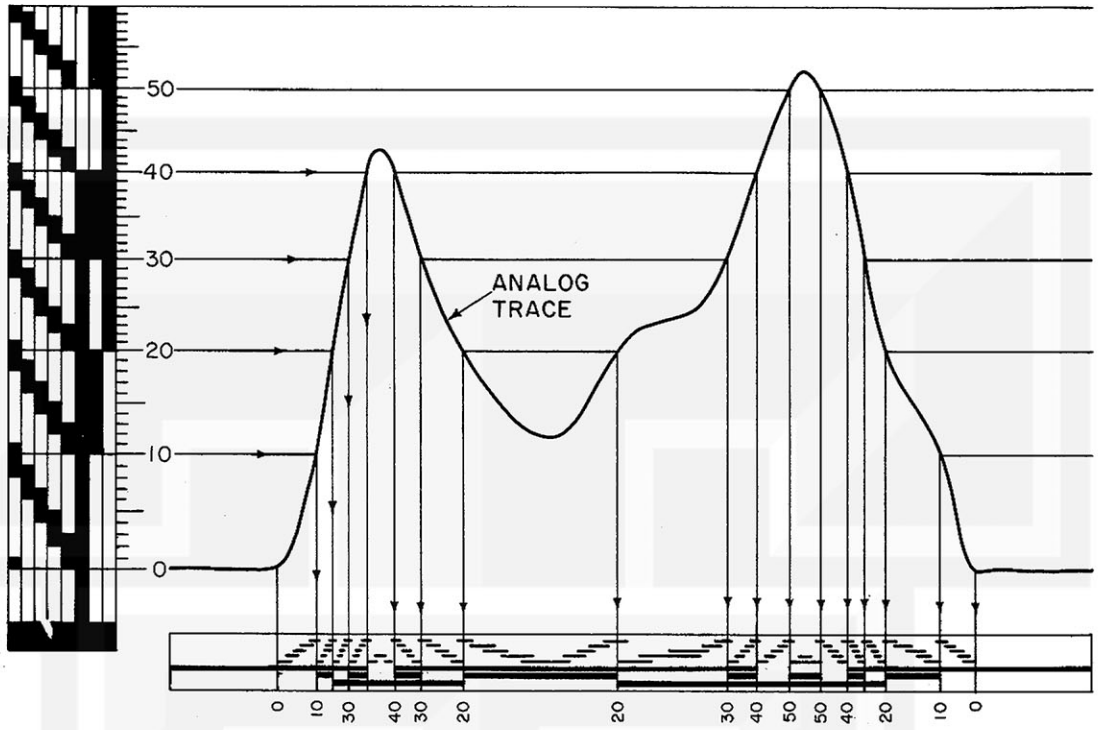

Fig. 13. Schematic diagram showing a portion of an analog trace which is coded and printed out within a narrow band. A printed circuit calibration board can be made to represent a given frequency-to-energy conversion curve.

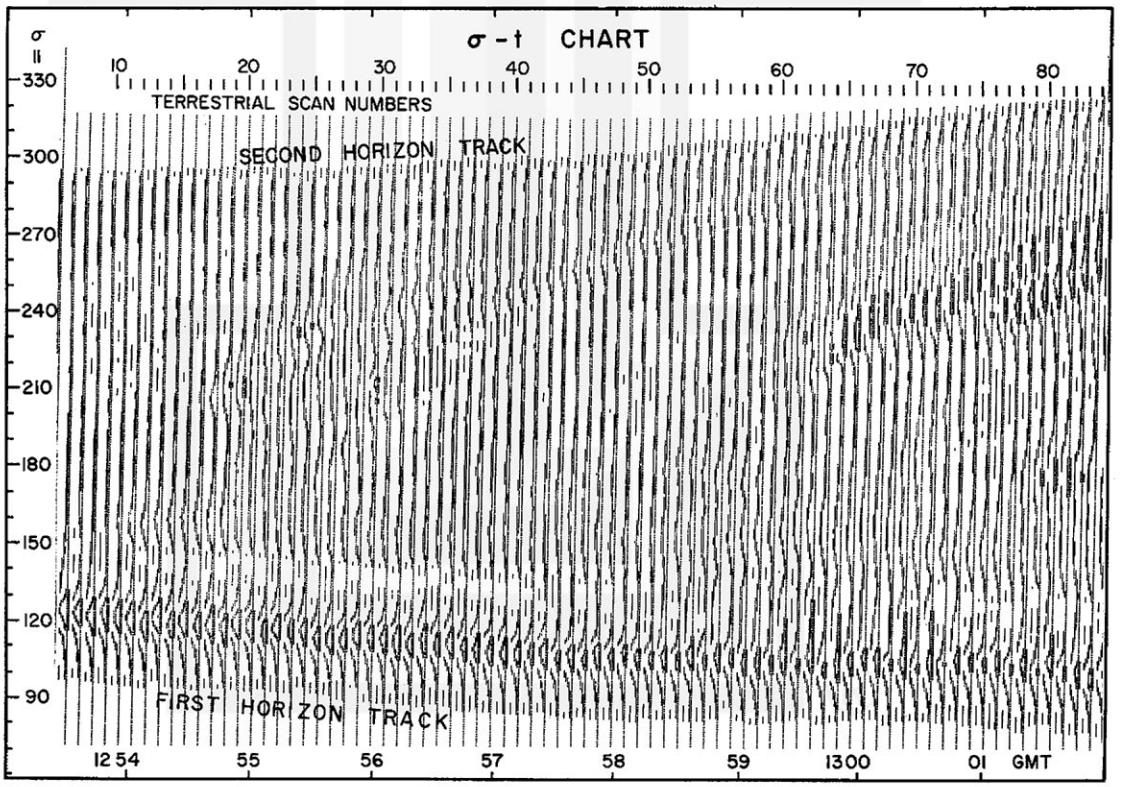

Fig. 14. An example of a coded radiation data printout by the Scanning Printer. On this printout chart, the scan angle (σ) increases upward, and the time toward the right. The coded notations on this chart represent unsmoothed calibrated radiation values read out directly from an analog trace.

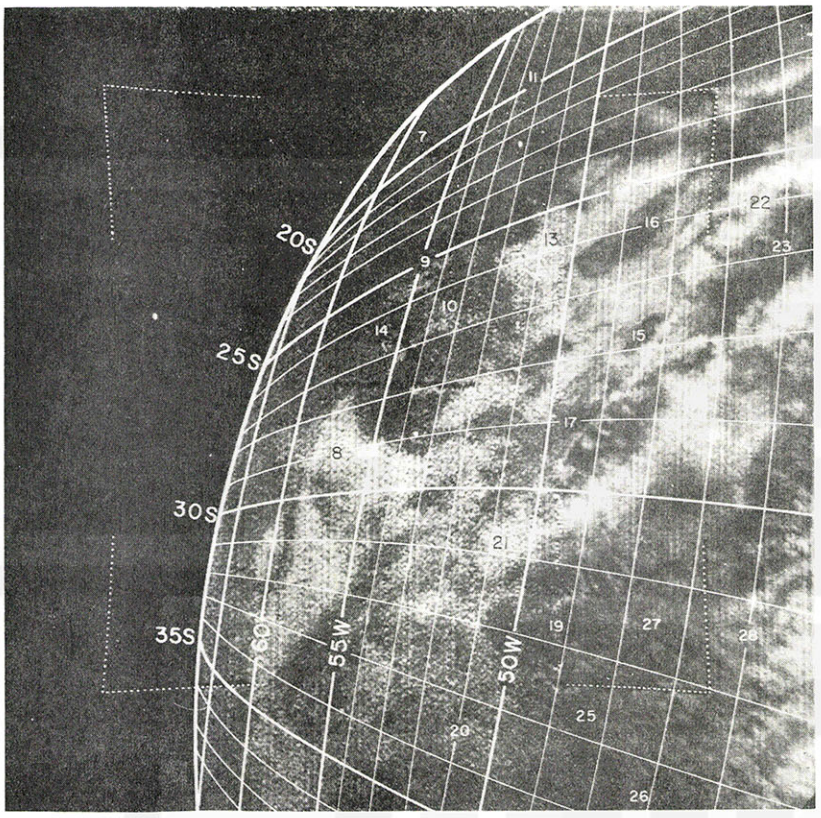

Fig. 15. Geographic grids and numbered significant points drawn on Frame 16T, which was exposed at 12h 56.9m, 1 August 1961, 767 km above 31.1S and 44.0W looking west with 50° tilt. The numbered points 15, 16, 17, and 21 are located along the Brazilian coast.

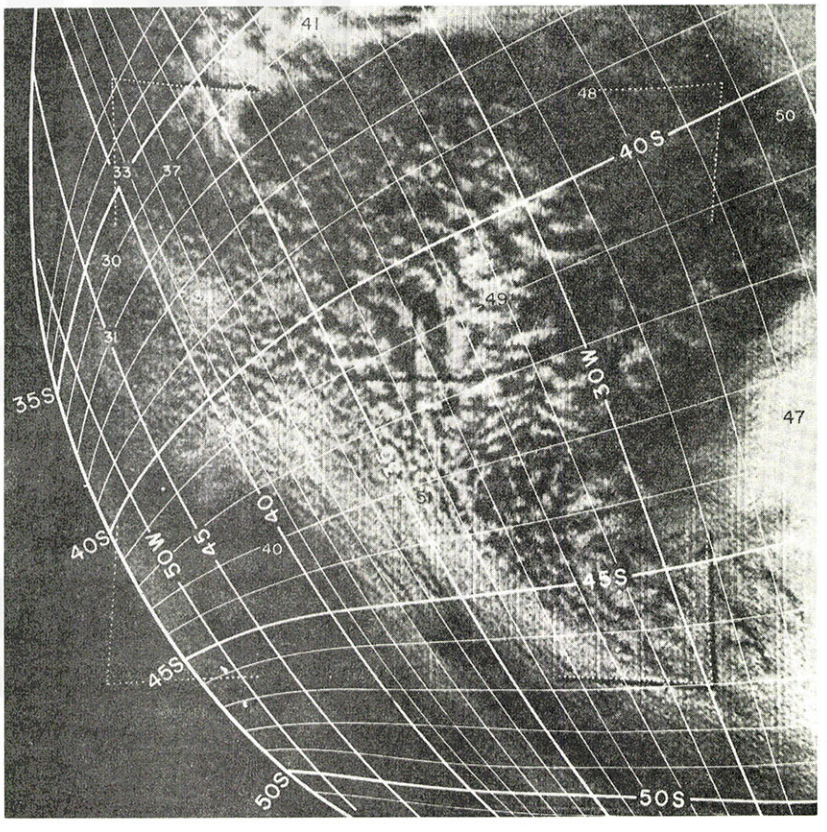

Fig. 16. Geographic grids and numbered significant points drawn on Frame 6T, exposed at 13h 01.0m, 1 August 1961, 811 km above 41.0S and 26.9W looking WSW with 35° tilt. No land areas are covered in this picture. Effective radiant emittance on Channel 2 indicates that the temperature of the cellular clouds near the picture center is about 20C colder than that of the underlying sea-surface.

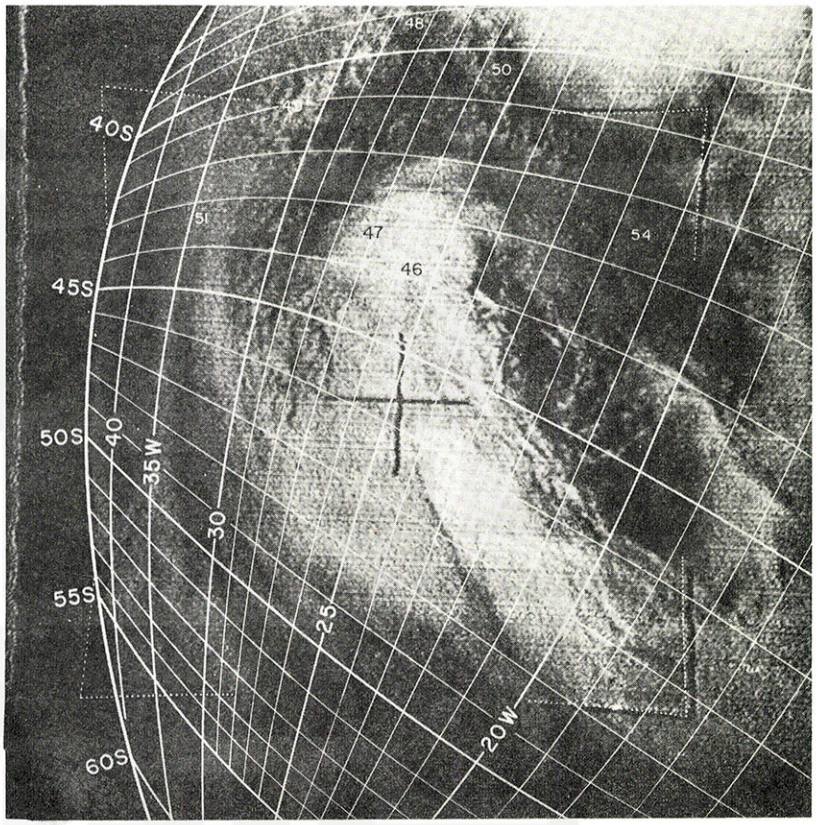

Fig. 17. Geographic grids and numbered significant points drawn on Frame 2T, exposed at 13 h 03.9m, 1 August 1961, 816 km above 43.9S, 18.5W looking WSW with 30° tilt. The numbered points 46 and 47 with their equivalent blackbody temperature -42C are located near the center of a south Atlantic cyclone. The cloud-free areas identified with numbers 48, 50, and 54 are about -7C which is 35C warmer than these clouds.

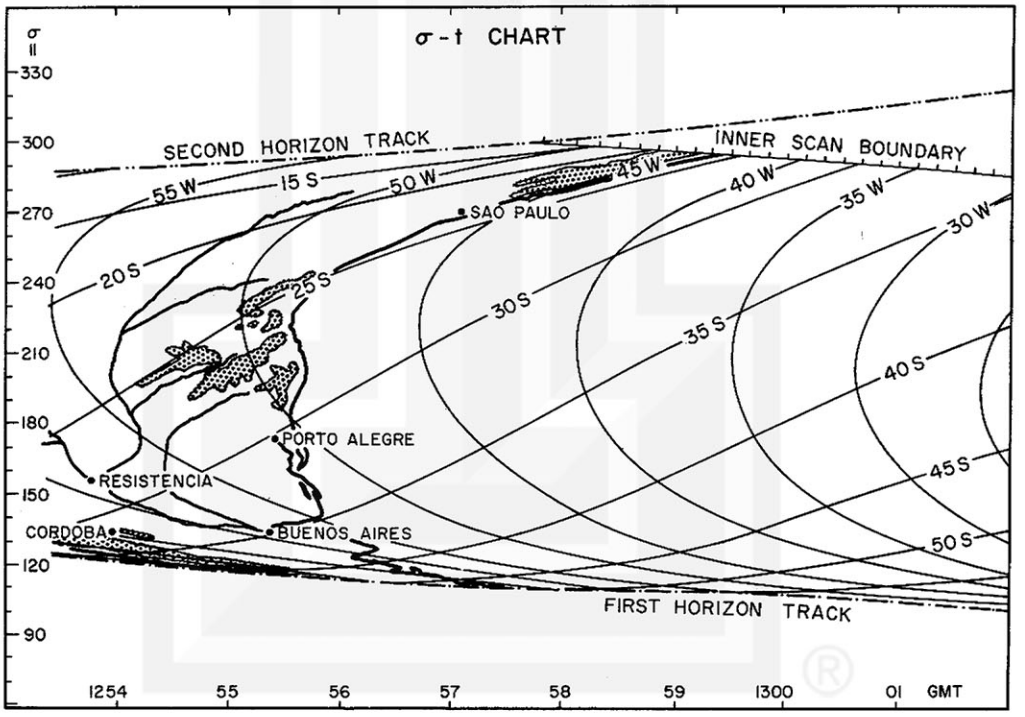

Fig. 18. Longitude and latitude lines drawn at 5° intervals to match the radiation printout chart which covers the area of Fig. 14. The coast of South America and main rivers are shown in heavy lines, and the areas above 1000 m are stippled. The scan angles of both longitudes and latitudes, which are required to construct these geographic grids, are now obtained graphically by using an OEC chart; these will be calculated by an electronic computer in the near future.

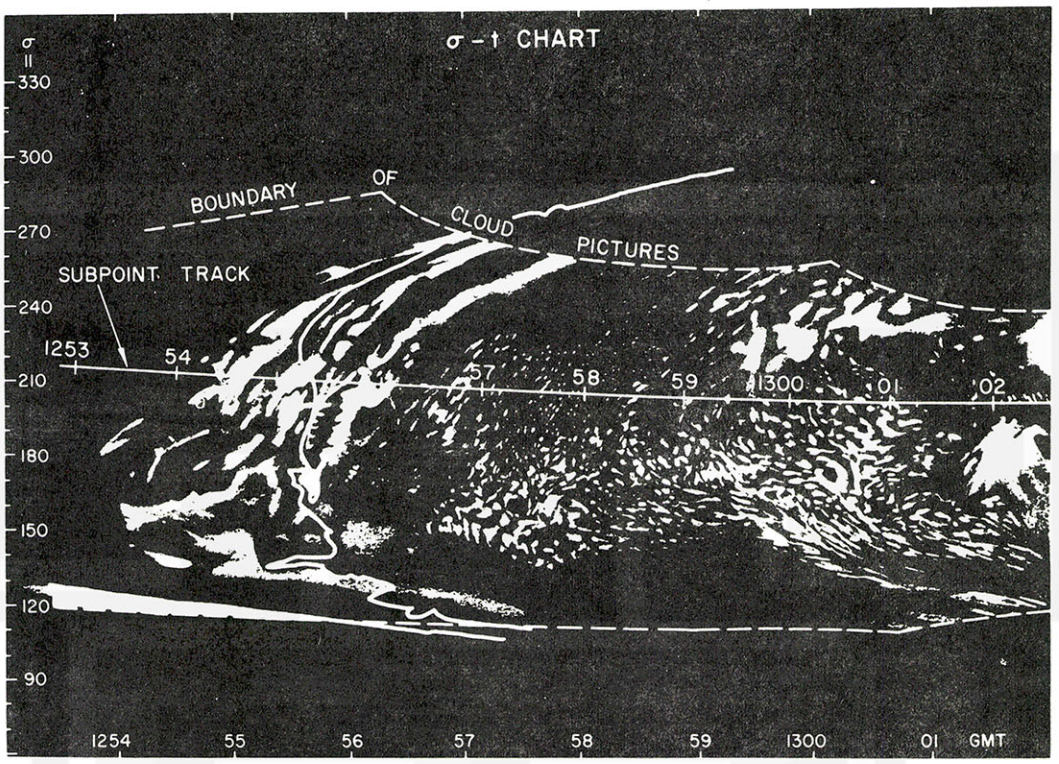

Fig. 19. Composite cloud patterns transcribed from several gridded photographs to the sigma-t printout coordinates. TIROS III Orbit 288, 1253-1302 GMT. This type of cloud chart is extremely useful in analyzing radiation patterns by superimposing a sigma-t printout chart.

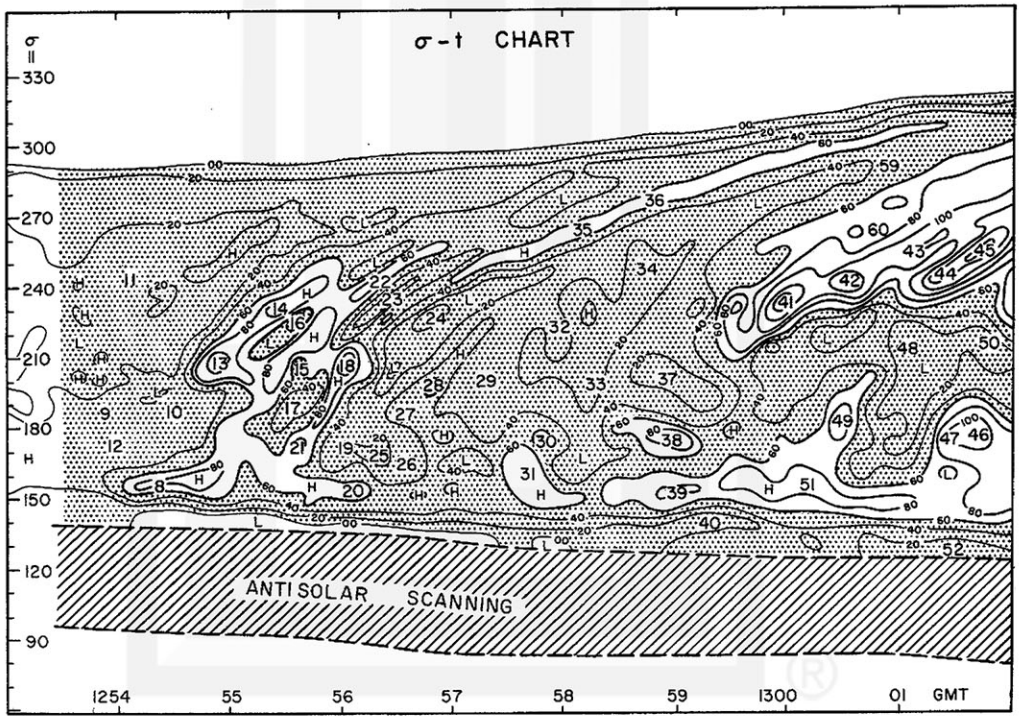

Fig. 20. Isolines of Channel 3 effective radiant emittance drawn on the sigma-t chart. Channel 3 values are contoured at 20 watts m^{-2} intervals. Ocean background shows practically zero value while Brazilian jungle reflects between 10 to 30 watts m^{-2} which gives few percent reflectance when divided by the effective incoming extra-terrestrial solar radiation.

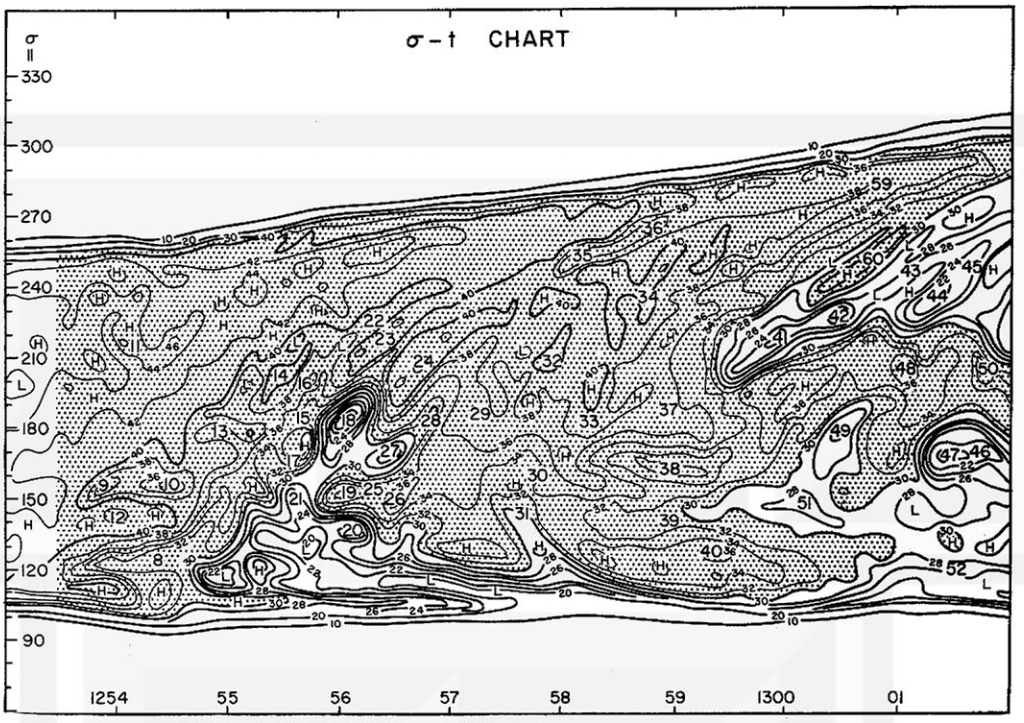

Fig. 21. Isolines of Channel 2 effective radiant emittance in watts m^{-2} drawn on a sigma-t chart. The areas with emittance above 30 watts m^{-2} are stippled. The same numbers representing significant points in Fig. 20 appear in this chart to permit direct comparison.

Fig. 22. Radiation contours of Channel 3 effective radiant emittance transferred onto Frame 11T. Such a transfer permits us to study the representativeness of radiation patterns in comparison with the photographic cloud covers. Note that the radiation contours depict average brightness from a group of clouds.

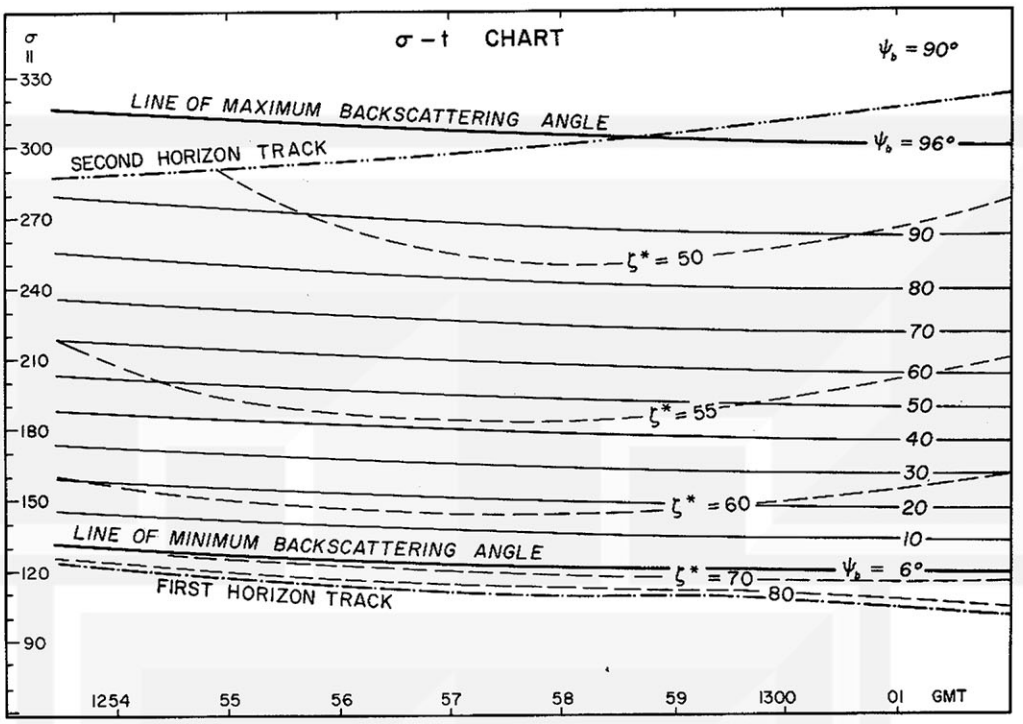

Fig. 23. Isolines of the solar zenith angles and the backscattering angles drawn on the sigma-t chart. The isolines of the backscattering angles are obtained by a computer whose output is the scan angles of given backscattering angles tabulated as a function of time. The solar zenith angles are determined as the distance between the TSS and the scan points on an OEC chart.

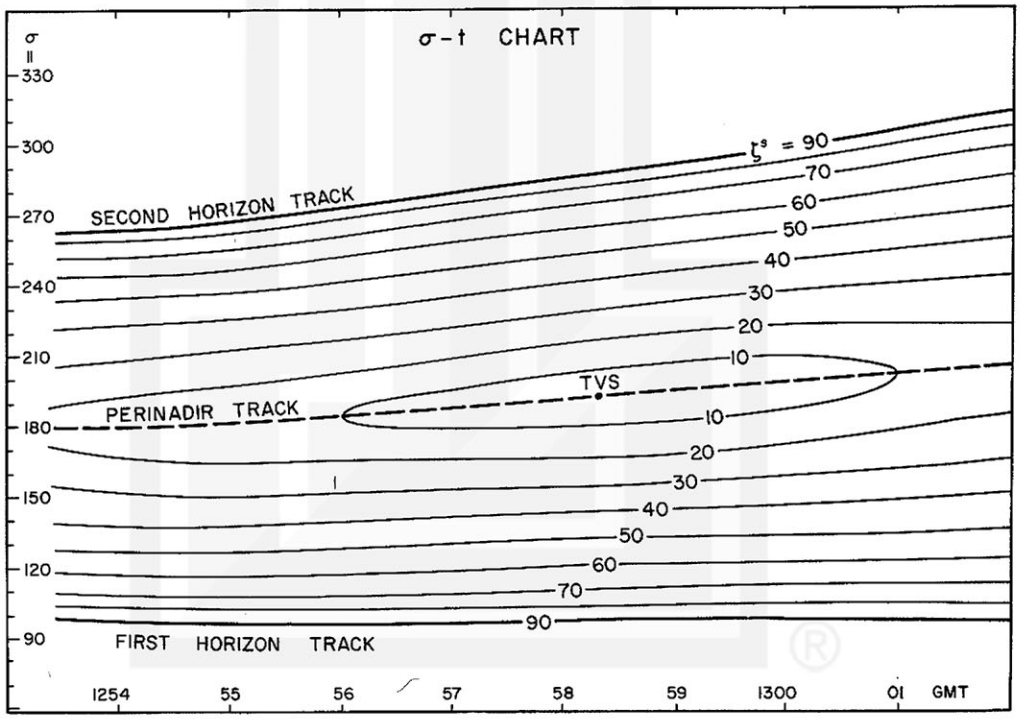

Fig. 24. Isolines of the zenith angle of the satellite drawn on the sigma-t chart. Because the scan angles representing a satellite zenith angle on a time line of a sigma-t chart are symmetric with respect to the perinadir, the construction of the isolines of a satellite zenith angle is extremely easy. A point TVS (vertical scan point) on the perinadir track is scanned with zero zenith angle.

MESOMETEOROLOGY PROJECT - - - - - RESEARCH PAPERS

(Continued from front cover)

16. Preliminary Result of Analysis of the Cumulonimbus Cloud of April 21, 1961 -Tetsuya Fujita and James Arnold

17. A Technique for Precise Analysis of Satellite Photographs - Tetsuya Fujita

18. Evaluation of Limb Darkening from TIROS III Radiation Data - S.H.H. Larsen, Tetsuya Fujita, and W.L. Fletcher

19. Synoptic Interpretation of TIROS III Measurements of Infrared Radiation -Finn Pedersen and Tetsuya Fujita

20. TIROS III Measurements of Terrestrial Radiation and Reflected and Scattered Solar Radiation - S.H.H. Larsen, Tetsuya Fujita, and W.L. Fletcher

21. On the Low-level Structure of a Squall Line - Henry A. Brown

22. Thunderstorms and the Low-level Jet - William D. Bonner

23. The Mesoanalysis of an Organized Convective System - Henry A. Brown

24. Preliminary Radar and Photogrammetric Study of the Illinois Tornadoes of April 17 and 22, 1963 - Joseph L. Goldman and Tetsuya Fujita

25. Use of TIROS Pictures for Studies of the Internal Structure of Tropical Storms -Tetsuya Fujita with Rectified Pictures from TIROS I Orbit 125, R/O 128 -Toshimitsu Ushijima

26. An Experiment in the Determination of Geostrophic and Isallobaric Winds from NSSP Pressure Data - William Bonner

27. Proposed Mechanism of Hook Echo Formation - Tetsuya Fujita with a Preliminary Mesosynoptic Analysis of Tornado Cyclone Case of May 26, 1963 -Tetsuya Fujita and Robbi Stuhmer

28. The Decaying Stage of Hurricane Anna of July 1961 as Portrayed by TIROS Cloud Photographs and Infrared Radiation from the Top of the Storm -Tetsuya Fujita and James Arnold

29. A Technique for Precise Analysis of Satellite Data, Volume II - Radiation Analysis, Section 6. Fixed-Position Scanning - Tetsuya Fujita

30. Evaluation of Errors in the Graphical Rectification of Satellite Photographs -Tetsuya Fujita

31. Tables of Scan Nadir and Horizontal Angles - William Bonner

32. A Simplified Grid Technique for Determining Scan Lines Generated by the TIROS Scanning Radiometer - James Arnold

33. A Study of Cumulus Clouds Over the Flagstaff Research Network with the Use of U-2 Photographs - Dorothy L. Bradbury and Tetsuya Fujita